Astron. Nachr. / AN **335**, No. 5, 543 – 548 (2014) / **DOI** 10.1002/asna.201412063

Local-density driven clustered star formation: Model and (some) implications

G. Parmentier⋆

Astronomisches Rechen-Institut, Zentrum für Astronomie der Universität Heidelberg, Mönchhofstr. 12-14, D-69120 Heidelberg, Germany

Received 2014 Apr 7, accepted 2014 Apr 10
Published online 2014 Jun 2

Key words ISM: clouds – galaxies: star clusters: general – stars: formation – stars: kinematics and dynamics

A positive power-law trend between the local surface densities of molecular gas, $\Sigma_{\rm gas}$, and young stellar objects, $\Sigma_{\rm stars}$, in molecular clouds of the solar neighbourhood has recently been identified. How it relates to the properties of embedded clusters has so far not been investigated. To that purpose, we model the development of the stellar component of molecular clumps as a function of time and local volume density. Specifically, we associate the observed volume density gradient of molecular clumps to the density-dependent free-fall time and we obtain the molecular clump star formation history by applying a constant star formation efficiency per free-fall time, $\epsilon_{\rm ff}$. The model reproduces naturally the observed ($\Sigma_{\rm gas}$, $\Sigma_{\rm stars}$) relation quoted above. The consequences of our model in terms of cluster survivability after residual star-forming gas expulsion and in terms of star age distribution in young gas-free clusters are discussed.

1 Introduction

The characterization of star-forming regions has made a significant leap forward thanks to the *Spitzer* Space Telescope. *Spitzer* has probed a wide spectrum of stellar densities in star-forming environments of the solar neighbourhood – from relative isolation to star clusters (although the Trapezium region of the Orion Nebula Cluster remains unresolved with that facility). In particular, recent observations by Heiderman et al.(2010) and Gutermuth et al.(2011) demonstrate that the efficiency of star formation is an increasing function of the gas surface density. Given that molecular clumps, the sites of star-cluster formation, are centrally concentrated (Beuther et al. 2002), this fact has profound implications for the formation of star clusters and their ability to survive the expulsion of their residual star-forming gas by massive-star activity.

A positive correlation between the gas density and the star formation efficiency arises naturally when star formation proceeds with a constant star formation efficiency *per free-fall time*, $\epsilon_{\rm ff}$, where the free-fall time is

$$\tau_{\rm ff} = \sqrt{\frac{3\pi}{32 G \rho_{\rm g}}} \, . \qquad (1)$$

In this class of models, molecular gas with a higher volume density, $\rho_{\rm g}$, – hence a shorter free-fall time, $\tau_{\rm ff}$ – forms stars more rapidly than gas with a low volume density (Krumholz & McKee 2005; Elmegreen 2011). This density-dependent star formation rate is akin to the density-dependent rate of star cluster dynamical evolution after gas expulsion studied by Parmentier & Baumgardt (2012).

This contribution summarizes the first steps of such a model which quantifies the building and properties of the stellar content of molecular clumps (Parmentier & Pfalzner 2013; Parmentier, Pfalzner & Grebel, subm.). As we shall see, combining the assumptions of a given star formation efficiency per free-fall time and spherical symmetry for molecular clumps allows to recover the star formation relation observed by Gutermuth et al. (2011). We discuss the model consequences for the density profile of the forming clusters, the growth with time of the star formation efficiency, and the size of star age spreads in clusters.

2 Model key facts

We assume (i) that the mass of molecular clumps is in place at the onset of star formation (Tackenberg et al. 2012), and (ii) that the clump remains in hydrostatic equilibrium for several free-fall times after the onset of star formation, that is, the clump is supported against gravity by, e.g., magnetic fields, turbulence, and protostellar outflows.

The volume density profile, $\rho_0(r)$, of a spherically symmetric molecular clump of mass M_0, radius R, and density index p_0, obeys

$$\rho_0(r) = \frac{3-p_0}{4\pi} \frac{M_0}{R^{3-p_0}} r^{-p_0} \, , \qquad (2)$$

where r is the distance from the clump centre. The subscript "0" refers to the gas properties prior to star formation (i.e. at $t = 0$: the clump is made of gas alone).

⋆ Corresponding author: gparm@ari.uni-heidelberg.de

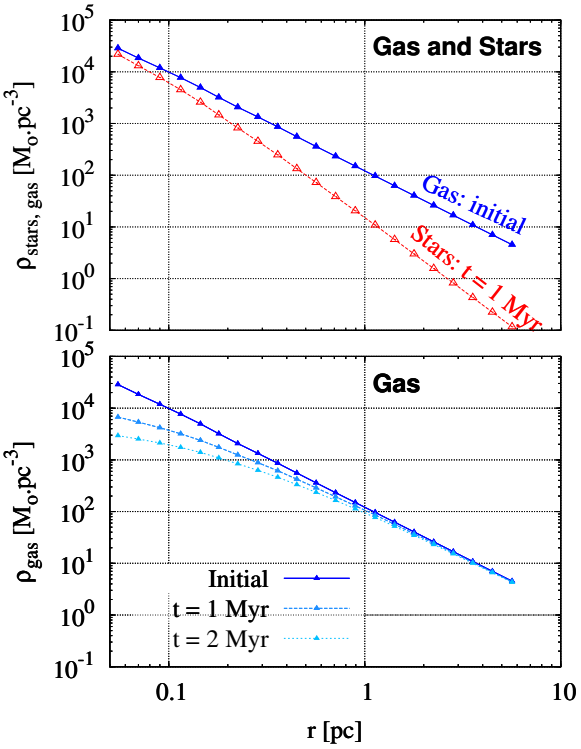

Fig. 1 *Top panel*: gas initial volume density profile (filled blue symbols) and the associated steeper stellar density profile (open red symbols) at $t = 1$ Myr. The spherical molecular clump has a mass $M_0 = 10^4\,\mathrm{M}_\odot$, a radius $R = 6$ pc, a density index $p_0 = 2$ and a star formation efficiency per free-fall time $\epsilon_{\rm ff} = 0.1$. *Bottom panel*: time evolution of the gas volume density profile. The faster star-formation-driven depletion of the gas in the central region of the molecular clump – where the free-fall time is the shortest – is clearly highlighted. (Adapted from Parmentier & Pfalzner 2013).

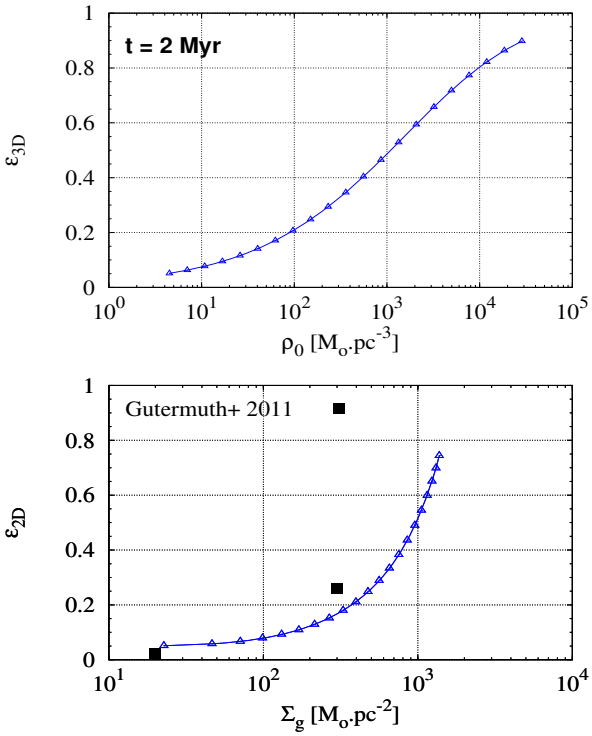

Fig. 2 *Top panel*: three-dimensional star formation efficiency, $\epsilon_{\rm 3D}$, as a function of the gas initial volume density ρ_0 at $t = 2$ Myr (model parameters as in Fig. 1). *Bottom panel*: same for the two-dimensional star formation efficiency, $\epsilon_{\rm 2D}$, as a function of the gas residual surface density. All quantities are defined locally, that is, at a given (3D: top; 2D: bottom) distance from the clump centre (Adapted from Parmentier & Pfalzner 2013).

If star formation obeys a constant star formation efficiency per free-fall time, $\epsilon_{\rm ff}$, then Eqs. (1) and (2) imply that star formation proceeds more quickly in the clump 's central regions than in its outskirts. This leads to a density profile for the stellar component that is steeper than the gas initially. The time evolution of the star- and gas-density profiles are solutions to separable first-order differential equations. These solutions obey (see Sect. 2.3 in Parmentier & Pfalzner 2013 for details)

$$\rho_g(t,r) = \left(\rho_0(r)^{-1/2} + \sqrt{\frac{8G}{3\pi}}\,\epsilon_{\rm ff}\,t\right)^{-2} \qquad (3)$$

and

$$\rho_\star(t,r) = \rho_0(r) - \rho_{\rm g}(t,r)\,, \qquad (4)$$

respectively. Examples of gas and star volume density profiles are shown in Fig. 1 (see the caption for the model parameters).

Note that, in this model, the free-fall time of the star-forming gas is defined locally and instantaneously as

$$\tau_{\rm ff}(t,r) = \sqrt{\frac{3\pi}{32G\rho_{\rm g}(t,r)}}\,, \qquad (5)$$

since the clump gas density profile is not uniform (Eq. 2) and the gas is depleted as time goes by.

With the gas turned into stars on a shorter time-scale in the clump inner regions than in the outer ones, the slope of the gas density profile gets shallower with time (see bottom panel of Fig. 1). It should therefore be kept in mind that gas density indices reported in the literature for star-forming molecular clumps may be shallower than the gas density index p_0 at the onset of star formation.

Based on the gas and star volume density profiles at time t, one can now define a local (i.e. radially-varying) star formation efficiency, $\epsilon_{3D}(t,r)$:

$$\epsilon_{\rm 3D}(t,r) = \frac{\rho_\star(t,r)}{\rho_\star(t,r)+\rho_{\rm g}(t,r)} = \frac{\rho_\star(t,r)}{\rho_0(r)}\,. \qquad (6)$$

By virtue of its dependence on the initial gas density, $\epsilon_{\rm 3D}(t,r)$ steadily decreases from the clump centre to the clump edge.

The three-dimensional star formation efficiency $\epsilon_{\rm 3D}(r)$ is not the star formation efficiency inferred by observers, however, since observers work with surface densities rather than volume densities. Therefore, building on the gas and star surface densities, we define a two-dimensional star formation efficiency as

$$\epsilon_{\rm 2D}(t,s) = \frac{\Sigma_{\rm stars}(t,s)}{\Sigma_{\rm stars}(t,s)+\Sigma_{\rm g}(t,s)} = \frac{\Sigma_{\rm stars}(t,s)}{\Sigma_0(s)}\,, \qquad (7)$$

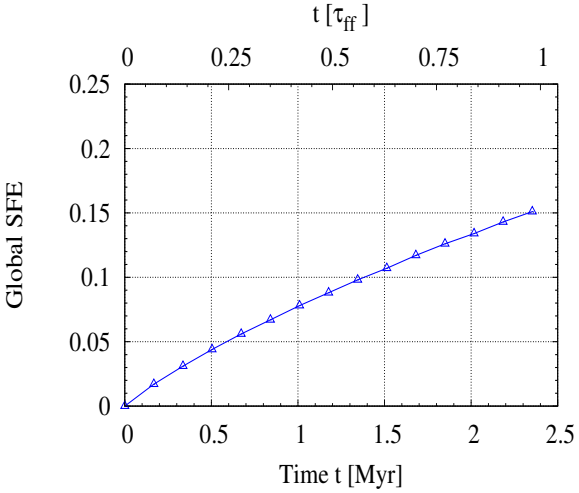

Fig. 3 Growth of the global star formation efficiency. Time is expressed in units of Myr and of the clump initial free-fall time on the bottom and top x-axes, respectively. The clump gas initial density profile has a slope of -2 and the star formation efficiency per free-fall time is $\epsilon_{\rm ff} = 0.1$. Note that, because of the gas central concentration, the SFE reaches a value of 16 %, rather than 10 %, within the first free-fall time of evolution.

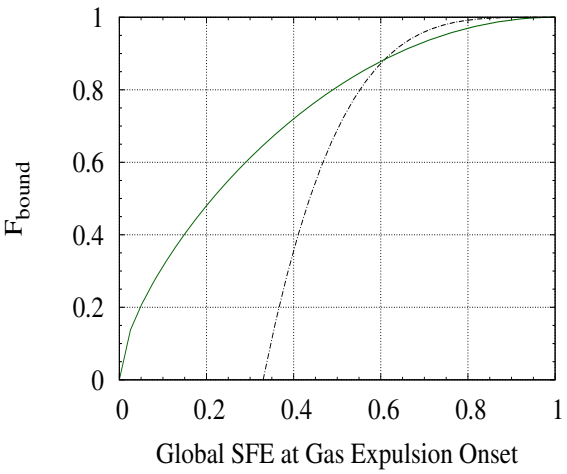

Fig. 4 Relation between the star mass fraction remaining bound to the cluster despite gas expulsion, F_{bound}, and the *global* SFE of the cluster-forming clump. The dash-dotted (black) line, taken from Parmentier & Gilmore (2007), corresponds to a uniform local star formation efficiency (i.e. $\epsilon_{\rm 3D}(r) = {\rm SFE}$ irrespective of r). The solid (green) line depicts a model from Adams (2000), with a radially-varying star formation efficiency (i.e. $\epsilon_{\rm 3D}(r)$ higher at smaller distance r from the clump centre). (Adapted from Parmentier & Pfalzner 2013).

where s is the projected distance from the clump centre.

The top panel of Fig. 2 illustrates the three-dimensional star formation efficiency as a function of the *initial* gas volume density (that is, the clump centre is now to the right side of the plot) at $t = 2$ Myr and for $\epsilon_{\rm ff} = 0.1$. The bottom panel depicts $\epsilon_{\rm 2D}$ in dependence of $\Sigma_{\rm g}$, the *residual* gas surface density. This is the parameter space mapped by observers. The measurements made by Gutermuth et al. (2011), $\epsilon_{\rm 2D} = 2.3\,\%$ and 26 % at $\Sigma_{\rm g} = 20$ and $300\,{\rm M}_\odot\,{\rm pc}^{-2}$, are also shown. Despite its simplifying assumptions (spherical symmetry and static distributions of the gas and newly formed stars), the model is in fair agreement with the observations.

Both $\epsilon_{\rm 3D}$ and $\epsilon_{\rm 2D}$ rise from a few per cent at the clump edge up to higher than 50 % at the clump centre. In particular, star formation depletes almost the entirety of the initial gas content in the clump centre, and $\epsilon_{\rm 3D}$ reaches values as large as 60–90 % in the inner $r \leq 0.1$ pc.

These high central values contrast with the low *global* star formation efficiency, SFE, namely the star formation efficiency averaged over the whole clump volume. Its evolution with time is shown in Fig. 3. The bottom and top x-axes show time expressed in units of 1 Myr and one clump initial free-fall time, respectively. At $t = 1$ Myr, the global SFE is only 8 %. Yet, as we shall see below, the cluster may survive the expulsion of its residual star-forming gas at such an early stage (see Sect. 3). Note that despite a star formation efficiency per free-fall time of 0.1, the global SFE reached at $t = \tau_{\rm ff,0}$ (equivalent here to $t = 2.4$ Myr) is 0.16. This is due to the free-fall time of the clump central regions being shorter than the clump mean free-fall time (see also Tan et al. 2006). Therefore, not only does the clump density gradient favour a higher star formation efficiency in the clump centre, it also speeds up star formation compared to a uniform-density clump (that is, ${\rm SFE}(t, p_0 > 0) > {\rm SFE}(t, p_0 = 0)$).

Attached is a movie illustrating the evolution with time of the gas density profile (left panel) and the evolution with time of the local three-dimensional star formation efficiency (right panel). Note that in the left panel, the x- and y-axes have logarithmic scalings, while they are linear in the right panel. Additional movies can be found at the following web site: http://wwwstaff.ari.uni-heidelberg.de/mitarbeiter/gparm/movies.html.

3 Star-cluster survival made easier

The expulsion of the residual star-forming gas out of newly formed clusters has often been presented as a key-stage of their evolution, which most of them do not survive (the so-called cluster infant mortality; e.g. Lada & Lada 2003). In the earliest models (instantaneous gas expulsion and negligible external tidal field; e.g. Lada, Margulis & Dearborn 1984), a cluster-forming clump must achieve a global star formation efficiency of at least one third for the cluster to survive gas expulsion. This result is illustrated as the dash-dotted black line in Fig. 4, where the x and y-axes represent, respectively, the global star formation efficiency at gas expulsion and the stellar mass fraction remaining bound to the cluster once the dynamical effects triggered by gas expulsion have faded away.

However, such models also build on a star formation efficiency which is uniform all through the cluster-forming molecular clump. This contrasts with the radially-varying star formation efficiency presented in Fig. 2. Let us consider

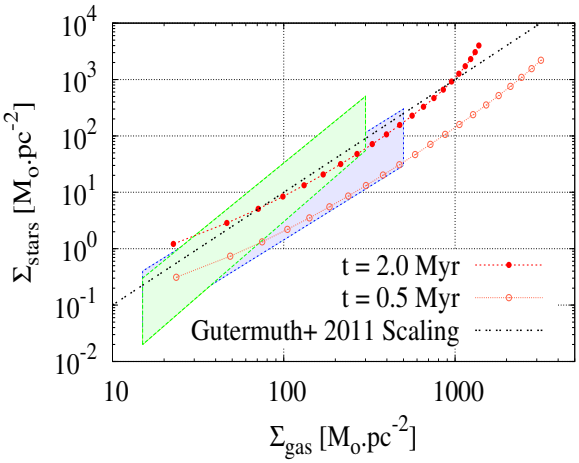

Fig. 5 Local surface density of YSOs, $\Sigma_{\rm stars}$, in dependence of the local surface density of the unprocessed/observed gas, $\Sigma_{\rm g}$ (same model parameters as in previous figures). The red lines with open/filled circles show the model predictions for the times t quoted in the key. The dotted (black) line depicts the mean star-formation relation inferred by Gutermuth et al. (2011). The blue and green polygons illustrate the scatter observed for the MonR2 and Ophiuchus molecular clouds, where it is the smallest. (Adapted from Parmentier & Pfalzner 2013).

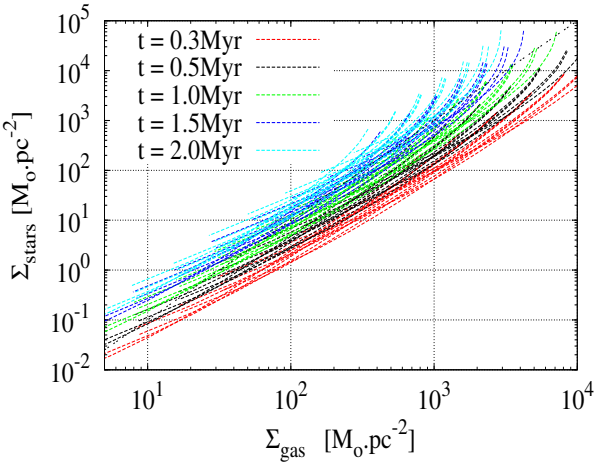

Fig. 6 Star formation relations for a number of molecular clumps displaying ranges of masses, radii and star-formation time-spans (see text for details)

a time $t = 1$ Myr after the onset of star formation. While the global SFE is low (SFE $\simeq 8\,\%$), the mean star formation efficiency in the inner 0.2 pc region is of order 50 % (see top panel of Fig. 1). So high a SFE in the clump centre implies a non-zero bound fraction of stars there after gas expulsion and, therefore, the global bound fraction cannot be zero either. As a result, even if the star formation efficiency averaged over the whole clump is significantly lower than 30 %, its locally high value in the clump central regions allows the cluster to survive gas expulsion as a bound – albeit depleted – stellar entity.

A pioneering semi-analytical study of this effect was carried out by Adams (2000). Its key-result is shown in Fig. 4 as the solid (green) line. It demonstrates how a centrally concentrated star-formation episode inflates star cluster survivability as compared to the case of a uniform star formation efficiency (compare the solid green and dash-dotted black lines).

4 The local star-formation relation

For a given molecular clump geometry, the volume density profiles of the gas and stars inferred in Sect. 2 can be transformed into their corresponding surface density profiles. One can then compare the star-formation relation predicted by the model to those observed for star-forming regions of the solar neighbourhood.

Figure 5 depicts the local surface density of young stellar objects (hereafter YSO), $\Sigma_{\rm stars}$, in dependence of the surface density of the observed/unprocessed gas, $\Sigma_{\rm g}$. Units are $\mathrm{M_\odot\,pc^{-2}}$ on both axes. The red lines with open and filled circles are the model predictions at $t = 0.5$ Myr and $t = 2$ Myr (same model parameters as in Fig. 1). The dotted (black) line shows the average star-formation relation inferred by Gutermuth et al. (2011) for a sample of molecular clouds of the solar neighbourhood:

$$\frac{\Sigma_{\rm stars}}{\mathrm{M_\odot\,pc^{-2}}} = 10^{-3}\left(\frac{\Sigma_{\rm g}}{\mathrm{M_\odot\,pc^{-2}}}\right)^2 . \quad (8)$$

The green and blue polygons illustrate the scatter of the observed relation for the Monoceros R2 and Ophiuchus molecular clouds, where it is the smallest.

The study of Gutermuth et al. (2011) encompasses mostly Class I protostars and Class II pre-main-sequence stars. Given that the respective average lifetimes of these phases are $\simeq 0.5$ Myr and $\simeq 2$ Myr (Evans et al. 2009), star formation in the regions they observed has been ongoing for presumably more than 1 Myr.

What is the star formation efficiency per free-fall time needed for the model to match the observed mean star-formation relation (Eq. 8) at, say, $t = 2$ Myr? We obtain $\epsilon_{\rm ff} = 0.1$ (value needed for the red line with filled circles to match the dotted black line in Fig. 5). We emphasize that this estimate of $\epsilon_{\rm ff}$ depends – in essence – on the assumed t-value. In other words, there is a degeneracy between the time-span since star formation onset (t) and the star formation efficiency per free-fall time ($\epsilon_{\rm ff}$). Should the lifetime of Class II objects be significantly longer than 2 Myr, as suggested by Bell et al. (2013), t may be substantially larger than 2 Myr in the regions mapped by Gutermuth et al. (2011). The derived star formation efficiency per free-fall time would accordingly be shorter. That could explain the one-order-of-magnitude difference between our $\epsilon_{\rm ff}$ estimate and that of Krumholz et al. (2012).

It is worth keeping in mind that Eq. (8) is an average. The observed YSO vs. gas surface – density relation exhibits a considerable scatter, even when plotted *per* molecular cloud (Gutermuth et al. 2011, their Fig. 9). Figure 5 illustrates as the blue and green parallelograms the scatter observed in the Monoceros R2 and Ophiuchus molecular clouds. Other molecular clouds exhibit an even greater

scatter. This scatter does not contradict the one-to-one relation predicted by the model since the latter quantifies the growth of the stellar mass per individual molecular *clump*. In contrast, a molecular *cloud* consists of *several clumps*, each with its own mass, radius, density index, and time-span since star formation onset. Therefore, a molecular cloud combines several star-formation relations, each with its own normalization. Summing up the contributions of a number of molecular clumps produces a scatter, which is depicted in Fig. 6. It shows the star-formation relation cumulated over a number of clumps, with masses ranging from 500 to $10^4\,\mathrm{M}_\odot$, radii from 1 to 4 pc, and times since star-formation onset from 0.5 to 2 Myr. This is therefore the star-formation relation which would be inferred for a molecular cloud consisting of such a collection of clumps. It is therefore unsurprising that the molecular clouds with the tightest star formation relations are those whose stellar content is dominated by a single molecular clump. In contrast, the Orion molecular cloud shows an extreme scatter due to the many non-coeval molecular clumps it consists of. Other reasons for the scatter in the observed $(\Sigma_\mathrm{g}, \Sigma_\mathrm{stars})$ relation include YSO migration, gas dispersal via stellar feedback processes, non-spherical molecular clumps and error measurements.

5 Star age spreads in young clusters

A natural outcome of this model is that the size of the stellar age spread in young clusters depends on the mean volume density of their gaseous progenitors. Actually, since star formation proceeds faster in denser gas, one expects dense molecular clumps to form clusters with narrow stellar age spreads. In what follows, we refer to the age spread of a cluster as the full width at half-maximum (FWHM) of its linear star age distribution, regardless of the shape of the distribution. This observed age spread is the imprint of the time taken by the star formation rate of the cluster-parent clump to drop to half its initial value. We emphasize that, as such, the age distribution FWHM differs from the duration of star formation, the latter being determined by the epoch of gas expulsion. Here we obtain and discuss the relation between star age spreads in clusters and the characteristics of cluster-parent clumps.

Figure 7 presents the star formation histories of two molecular clumps. Clump A has a mass $M_0 = 6\times10^4\,\mathrm{M}_\odot$ and a radius $R = 0.5\,\mathrm{pc}$, Clump C has a mass $M_0 = 4000$ $\mathrm{M}_\odot$ and a radius $R = 2\,\mathrm{pc}$. Their mean volume densities differ by three orders of magnitude and their mean free-fall time by a factor 30. The top panel shows the evolution with time of the star formation rate. As star formation depletes the clump gas reservoir, the gas free-fall time steadily increases and the star formation efficiency per free-fall time is applied to an ever lower gas mass. Therefore, unless the clump contracts or is replenished in gas by inflows, the star formation rate decreases with time. This decrease is faster in high-density regions (here Clump A) since – in essence – they evolve on a faster time-scale. The bottom panel of

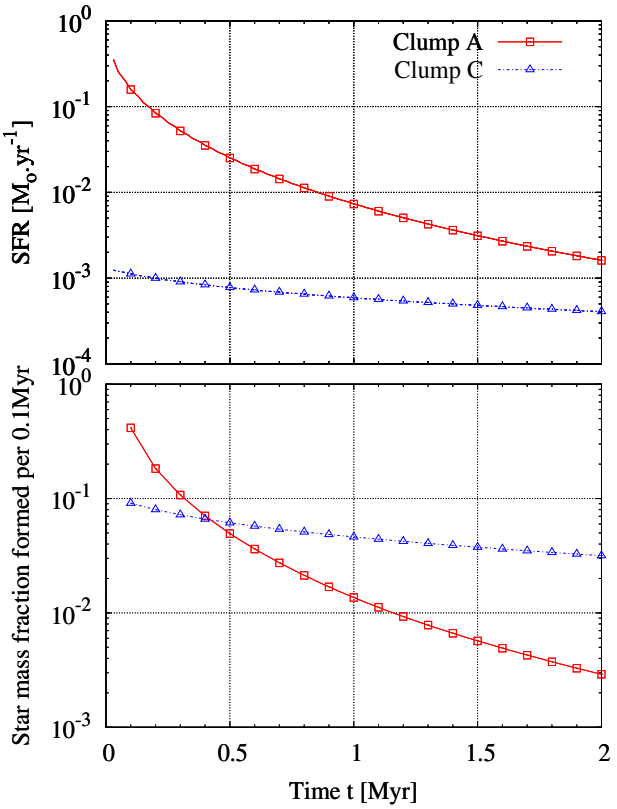

Fig. 7 *Top panel*: evolution with time of the star formation rate of two molecular clumps whose mean volume densities differ by three orders of magnitude. Both gas density profiles are isothermal spheres initially (i.e. $p_0 = 2$), with a central flat core ($r_\mathrm{c} = 0.01$ pc) and the star formation efficiency per free-fall time is $\epsilon_\mathrm{ff} = 0.1$. *Bottom panel*: for the same clumps, evolution with time of the star mass fraction formed per 0.1 Myr. The mass fraction is defined with respect to the total stellar mass formed 2 Myr after star formation onset.

Fig. 7 depicts the time evolution of the stellar mass fraction formed per constant time-interval $\Delta t = 0.1\,\mathrm{Myr}$. The mass fractions are defined with respect to the clump stellar mass at $t_\mathrm{end} = 2\,\mathrm{Myr}$. Figure 7 shows that Clump A builds $\simeq 40\,\%$ of its final stellar mass within the first $0.1\,\mathrm{Myr}$, whereas after one million years, the mass fraction added to the stellar content per 0.1,Myr has dropped to a mere 1 %. In contrast, Clump C forms at any time 3–10 % of its final stellar mass per time-interval of 0.1 Myr. Figure 7 clearly illustrates the ability of high-density regions (Clump A) to undergo rapid star formation episodes.

One can quantify how fast the star formation rate declines with time based on its half-life time, $t_{1/2}$, namely, the time needed for it to drop to half its initial value. Along with the bin size and the age error, this half-life time will strongly influence the FWHM of the linear stellar age distribution. It is illustrated in Fig. 8 where the star formation histories of Clumps A and C have been normalized to their initial value. Half the initial star formation rate is indicated by the horizontal dashed line. One can see that the half-life

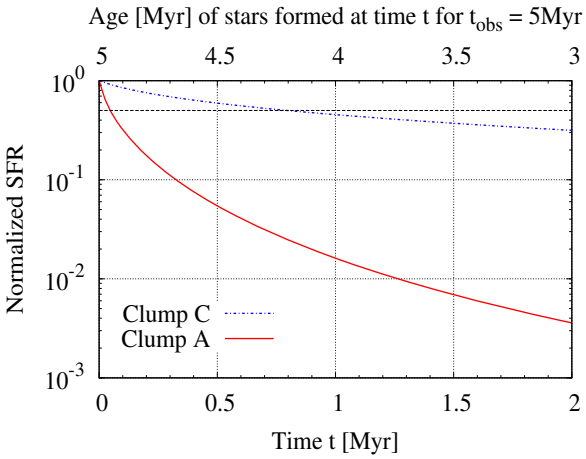

Fig. 8 Evolution with time of the star formation rate normalized to its initial value for the same molecular clumps as in Fig. 7. The bottom x-axis gives the time elapsed since the onset of star formation. The top x-axis corresponds to the age of the newly-formed stars if the cluster is observed 5 Myr after star formation onset. The horizontal dashed black line shows half the initial star formation rate, allowing therefore a direct read of the half-life time, $t_{1/2}$, of the star formation rate.

time of Clump A is about 0.05Myr, and that of Clump C is about 0.8 Myr.[1]

Not only does the half-life time depend on the clump mean density, it also depends on the adopted star formation efficiency per free-fall time. A lower $\epsilon_{\rm ff}$-value decreases the rate of star formation and slows down its evolution in time (since the gas is depleted on a longer time-scale). For $\epsilon_{\rm ff} \simeq 0.01$, the half-life time of the star formation history is an order of magnitude longer than found in Fig. 8. Here there is therefore a degeneracy between the clump mean volume density and the star formation efficiency per free-fall time. Should the star formation efficiency per free-fall time be reasonably known (but see the caveat above regarding the Class-II phase duration), the half-life time $t_{1/2}$ of the clump star formation rate could be used as a probe into the clump mean density.

An exciting prospect is thus emerging here. Since the half-life time $t_{1/2}$ leaves an imprint onto the FWHM of the observed star age distribution of a young gas-free cluster, it may be doable to infer the mean volume density of the cluster progenitor from its observed star age distribution (Parmentier, Pfalzner & Grebel 2014). One expects denser molecular clumps to give rise to clusters with narrower stellar age distributions, an effect which seems to have been unveiled recently (Kudryavtseva et al. 2012). Note that the mean volume density of young clusters differs from that of their parent clumps because of the post-gas-expulsion cluster expansion and mass-loss. It therefore remains to be seen whether the anticipated correlation between the star age distribution FWHM and the clump mean volume density survives when one considers the mean volume density of young gas-free star *clusters*.

[1] It should be noted that, to avoid a singularity at the centre of our model clumps, a power-law density profile with a central flat core has been adopted (here $r_{\rm c} = 0.01$ pc). This is the presence of this flat core which prevents the half-life time to scale exactly as the clump free-fall time. That is, the ratio between the half-life time of Clumps C and A (0.8 Myr/0.05 Myr $\simeq$ 16) is not exactly the factor 30 found between their respective free-fall times.

6 Conclusions

We have presented a model quantifying the stellar content of molecular clumps as a function of time and initial gas volume density. The model key ingredient is the star formation efficiency per free-fall time, $\epsilon_{\rm ff}$, namely, the mass fraction of gas turned into stars per free-fall time, $\tau_{\rm ff}$ (Eq. 1). In this class of models, the star formation efficiency increases more rapidly in higher volume-density gas than in low volume-density gas. Model consequences are:

- the star-formation relation ($\Sigma_{\rm gas}$, $\Sigma_{\rm stars}$) of cluster-forming clumps has a slope steeper than unity as is observed;
- the ability of star clusters to survive the expulsion of their residual star-forming gas is strengthened owing to the locally high star formation efficiency in the inner parts of cluster-forming clumps;
- dense molecular clumps give rise to star clusters with narrow stellar age spreads.

Acknowledgements. G.P. thanks the Organising Committee of the Astronomische Gesellschaft 2013 annual meeting for the invitation to present her research in plenary session and the Zentrum für Astronomie der Universität Heidelberg for having proposed her name. This work has been supported by a Research Fellowship of the Max-Planck-Institut für Radioastronomie (Bonn), and an Olympia-Morata Fellowship of Heidelberg University.

References

Adams, F. 2000, ApJ, 542, 964
Bell, C.P.M., Naylor, T., Mayne, N.J., Jeffries, R.D., & Littlefair, S.P. 2013, MNRAS, 434, 806
Beuther, H., Schilke, P., Menten, K.M., et al. 2002, ApJ, 566, 945
Elmegreen, B.G.: 2011, ApJ, 731, 61
Evans, N.J. II, Dunham, M.M., Jörgensen, J.K., et al. 2009, ApJS, 181, 321
Gutermuth, R.A., Pipher, J.L., Megeath, S.T., et al. 2011, ApJ, 739, 84
Heiderman, A., Evans, N.J. II, Allen, L.E., Huard, T., & Heyer, M. 2010, ApJ, 723, 1019
Krumholz, M.R., & McKee, C.F. 2005, ApJ, 630, 250
Krumholz, M.R., Dekel, & A.,McKee, C.F. 2012, ApJ, 745, 69
Kudryavtseva, N., Brandner, W., Gennaro, M., et al. 2012, ApJ, 750, L44
Lada C.J., & Lada E.A. 2003, ARA&A, 41, 57
Lada, C.J., Margulis, M., & Dearborn, D. 1984, ApJ, 285, 141
Parmentier, G., & Gilmore G. 2007, MNRAS, 377, 352
Parmentier, G., & Baumgardt, H. 2012, MNRAS, 427, 1940
Parmentier, G., & Pfalzner, S. 2013, A&A, 549, 132
Parmentier, G., & Pfalzner, S., & Grebel E.K. 2014, ApJ, subm.
Tackenberg, J., Beuther, H., Henning, T., et al. 2012, A&A, 540, 113
Tan, J.C., Krumholz, M.R., & McKee, C.F. 2006, ApJ, 641, L121

